RSC Sustainability

ROYAL SOCIETY OF CHEMISTRY

PAPER

View Article Online
View Journal | View Issue

Cite this: *RSC Sustainability*, 2025, **3**, 4759

Visible-light-induced photocatalytic oxidation of C–H bonds with O_2 employing simple porphyrins as photocatalysts under solvent-free conditions

Yan-Bo Ding, Yi-Lin Chu, Qiu-Ping Liu, Hong-Ke Wu, Hai-Min Shen * and Yuan-Bin She*

To insert oxygen atoms into C–H bonds through efficient and green process with lower energy consumption and lower carbon emission, porphyrins and metalloporphyrins as model compounds of chlorophyll were utilized as photocatalysts and applied to the oxidation of C–H bonds with O_2 under irradiation of visible light at room temperature and solvent-free conditions. The generation efficiency of oxygen-containing products reached up to the millimolar level (mmol ($g_{cat.}^{-1}$ h^{-1})) with excellent substrate tolerance. In cyclohexane oxidation as the model reaction, substrate conversion reached up to 3.18 mmol ($g_{cat.}^{-1}$ h^{-1}) with a selectivity of 99.9% towards cyclohexyl hydroperoxide, utilizing optimized tetrakis(4-carboxyphenyl)porphyrin (T(4-COOH)PP) as the photocatalyst. Based on characterization studies of UV-vis absorption spectroscopy, photoluminescence emission spectroscopy, time-resolved photoluminescence spectroscopy, transient photocurrent spectroscopy and electrochemical impedance spectroscopy, the source of excellent catalytic performance of T(4-COOH)PP was investigated, and it was ascribed to its higher performance in visible-light absorption, charge separation, production of photo-generated electrons, and lower impedance during charge migration under irradiation of visible light. The reactive species and reaction mechanism in this work were investigated in detail as well. The production efficiency of oxidation products at the millimolar level (mmol ($g_{cat.}^{-1}$ h^{-1})) was higher than most of the reports in current literature. Thus, the oxidation method developed in this work was an efficient, sustainable and low-energy consumption strategy for oxidative functionalization of C–H bonds and would be a valuable reference for the development of an efficient, sustainable, low-energy consumption and low-carbon emission chemical process.

Received 23rd June 2025
Accepted 18th August 2025

DOI: 10.1039/d5su00471c

rsc.li/rscsus

Sustainability spotlight

Through learning from nature, this work presents a green and sustainable C–H bond oxidation strategy utilizing renewable visible light as the energy source under solvent-free and room temperature conditions, which is a low-energy consumption and low-carbon emission chemical process. The generation efficiency of oxygen-containing products in C–H bond oxidation with O_2 irradiated under visible light reached up to the millimolar level (mmol ($g_{cat.}^{-1}$ h^{-1})) and was higher than most of the reports in current literature. The substrate conversion in cyclohexane oxidation as a model reaction reached up to 3.18 mmol ($g_{cat.}^{-1}$ h^{-1}) with a selectivity of 99.9% towards cyclohexyl hydroperoxide, providing an efficient and sustainable C–H bond oxidation route with high atom economy. Furthermore, the strategy developed in this work will be further enhanced through constructing a cascade catalytic system to regulate the range of oxidation products and generation efficiency and act as a valuable reference for the realization of sustainable development, green chemistry and energy conservation & emission reduction in the chemical industry.

1. Introduction

In the chemical industry and related academic research, direct oxidative functionalization of C–H bonds using molecular oxygen (O_2) has always been regarded as a promising, efficient and rational strategy to utilize the abundant and cheap hydrocarbons in the petroleum industry, through which various bulk chemicals and fine chemical intermediates can be obtained with the shortest reaction route and highest atom economy.[1–5] In these important oxidative transformations, the most critical step is the insertion of oxygen atoms into C–H bonds to form alkyl hydroperoxides, which are the main oxidation intermediates in hydrocarbon oxidation with O_2 and can be transformed into a series of valuable and useful oxygen-containing compounds.[6–8] However, because of the higher dissociation energy (typically more than 300 kJ mol^{-1})[5,9–12] and lower polarity of C–H bonds[11–13] and the inertness of triplet ground-state of O_2,[12,14] the oxidation of C–H bonds with O_2 usually required the

College of Chemical Engineering, Zhejiang University of Technology, Hangzhou 310014, China. E-mail: haimshen@zjut.edu.cn; Tel: (+86)159-8846-0002

reaction temperature reaching up to more than 130 °C,[2,9,15] resulting in very high energy consumption and carbon emissions, which is inconsistent with the principles of green chemistry.[16–18] A representative example is the oxidation of cyclohexane with O_2 to produce KA oil (a mixture of cyclohexanone and cyclohexanol), which are important intermediates of industrial manufacture of polyamide fibers.[1,3,19–21] The industrial oxidation of cyclohexane with O_2 is usually conducted in the temperature range of 150–170 °C.[8–10,22,23] The higher reaction temperatures not only result in higher energy consumption but also increase the carbon emissions, which is contrary to the demand for energy conservation & emission reduction and sustainable development in the chemical industry. Thus, to realize the oxidation of C–H bonds with O_2 through an energy conservation route is an urgent demand for constructing green and sustainable chemical processes with lower energy consumption and lower carbon emissions.

Photocatalysis, especially employing visible light as an energy source, has often been adopted as a green, sustainable, low-energy, and low-emission strategy to solve the problems in traditional thermal catalysis.[24–26] In visible-light-induced photocatalysis, not only the abundant solar energy can be employed as a potential energy source but also the catalytic transformation can be carried out at room temperature. Therefore, the visible-light-induced photocatalytic technology has also been introduced to the oxidation of C–H bonds with O_2 to solve the high energy consumption and high carbon emission.[20,25,27–31] To effectively utilize the energy of visible light to activate C–H bonds and O_2 and realize the insertion of oxygen atoms into C–H bonds, a series of ingenious and efficient photocatalysts were developed and applied, such as titanium dioxide (TiO_2)-based catalysts,[25–27,32] bismuth (Bi)-based catalysts,[20,33–35] tungsten (W)-based catalysts,[29,34,35] cerium (Ce)-based catalysts,[36,37] perovskite-based catalysts[30,38] and so on. Benefiting from the efficient photocatalysts, oxygen atoms were inserted into C–H bonds successfully at room temperature in the presence of visible light, and usually the oxygen-containing products could be obtained at a micromolar level (μmol ($g_{cat.}^{-1}$ h^{-1})).[20,25,27–31] With the great achievement in inserting oxygen atoms into C–H bonds, the next problem that must be solved is to boost the conversion efficiency. Compared with traditional thermal catalysis, the conversion efficiency in oxidation of C–H bonds through visible-light-induced photocatalysis is still at a lower level, usually being far below 1%,[20,25,27–31] which inhibited the extensive application of visible-light-induced photocatalytic technology in industrial oxidative functionalization of C–H bonds seriously.

To further enhance the utilization efficiency of visible light and promote the insertion of oxygen atoms into C–H bonds, the discovery and development of efficient photocatalytic materials remain the work focus in photocatalytic C–H bond oxidation. As for the efficient catalytic materials in utilization of visible light, chlorophyll in plants is definitely the best and ideal choice, which plays a vital role in the chemical transformations within living organisms employing visible light as the energy source.[39–41] In regard to the chemical structure, the most representative feature of chlorophyll is the highly conjugated quaternary porphyrin ring, which can absorb the solar energy efficiently and store it in biomass.[41,42] Therefore, porphyrins and their metal complexes (metalloporphyrins) have frequently been employed as model compounds of chlorophyll and heme and applied in catalysis chemistry to promote various chemical transformations.[43–46] In addition, inspired by the high efficiency of chlorophyll in utilizing visible light to promote chemical transformations and adhering to the principle of learning from nature, simple porphyrins and metalloporphyrins were employed as model compounds of chlorophyll to initiate visible-light-induced photocatalytic oxidation of C–H bonds with O_2 in this work based on our precious research studies.[47–54] It is very exhilarating that, when porphyrins were employed as photocatalysts, not only the insertion of oxygen atoms into C–H bonds induced by visible light was realized at room temperature but also the generation efficiency of oxidation products reached up to the millimolar level (mmol ($g_{cat.}^{-1}$ h^{-1})) with excellent substrate tolerance. For the optimized tetrakis(4-carboxyphenyl)porphyrin (T(4-COOH)PP) photocatalyst, the yield of oxygen-containing products in the typical oxidation of cyclohexane reached up to 3.18 mmol ($g_{cat.}^{-1}$ h^{-1}) with a selectivity of 99% towards cyclohexyl hydroperoxide ($C_6H_{11}OOH$) (Scheme 1). Through photoelectrochemical performance tests and mechanism research studies, the origin of the outstanding photocatalytic property of T(4-COOH)PP was explored as its stronger visible-light absorption ability, higher separation efficiency of photogenerated electrons–holes, lower recombination of the generated electrons–holes and higher electron transport capacity. Considering the yield of oxidation products at the millimolar level (mmol ($g_{cat.}^{-1}$ h^{-1})), not only efficient insertion of oxygen atoms into C–H bonds was realized when induced by visible light at room temperature in this work but also a successful example was provided for the achievement of efficient chemical transformation through learning from nature. Thus, this work will act as an inspiring, rational and practical reference for both the industrial oxidation of C–H bonds and development of other efficient, sustainable, low-energy consumption, low-carbon emission catalytic processes, eventually promoting the realization of green chemistry, energy conservation & emission reduction and sustainable development in the chemical industry.

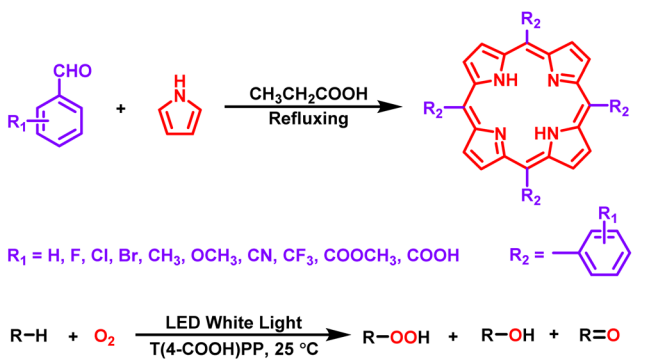

Scheme 1 Syntheses of porphyrins and photocatalytic oxidation of C–H bonds with O_2.

2. Experimental section

Chemical reagents and materials, characterization studies and instruments are presented in the SI.

2.1. Syntheses of porphyrins and metalloporphyrins

Porphyrins and metalloporphyrins utilized in this work as photocatalysts were synthesized according to the procedures reported in our previous studies.[51–59] All the obtained porphyrins and metalloporphyrins were purified through column chromatography and determined through comparison with standard samples in our laboratory utilizing thin layer chromatography. Porphyrins and metalloporphyrins utilized as photocatalysts in this work were also characterized and determined through ^{1}H NMR spectroscopy, ^{13}C NMR spectroscopy, ESI-MS and FT-IR spectroscopy, and the corresponding characterization spectra are presented in the SI.

2.2. Photocatalytic oxidation of C–H bonds with O_2

Photocatalytic oxidation of C–H bonds with O_2 was carried out following the procedure below utilizing cyclohexane as a model substrate. In a glass reaction tube with a branch pipe and a high vacuum valve (25 mL), porphyrin or metalloporphyrin (5×10^{-3} mmol) was dispersed in cyclohexane (4.2080 g, 50 mmol), and the reaction tube was sealed with an oxygen balloon (1 atm). After stirring at 25 °C for 10 min, the reaction mixture was irradiated with visible light for a certain reaction time utilizing a LED white light lamp in a certain wattage as the light source. And the distance between the reaction tube and visible-light source was 4 cm. When the reaction was completed, triphenylphosphine (1.0492 g, 4 mmol) was added to the resultant reaction mixture with continued stirring for 15 min to transform the formed hydroperoxide. All the reaction mixture was transferred to a volumetric flask (25 mL), dissolved and made up to 25 mL exactly with acetone as the solvent. One portion of acetone solution (10 mL) was utilized to conduct GC analyses to determine the yield of the partial oxidation products with toluene (0.0921 g, 1 mmol) as the internal standard. Another 10 mL of acetone solution was utilized to conduct HPLC analyses to determine whether there was overoxidation products like alkyl dicarboxylic acid in the reaction mixture. Considering the volatility of hydrocarbons and its effect on substrate conversion, the substrate conversion and selectivity to oxidation products in photocatalytic oxidation of C–H bonds were calculated following **eqn (1)** and **(2)**.

$$\text{Conversion}(\%) = \frac{\text{Moles of all oxidation products}}{\text{Initial moles of substrate}} \times 100\% \quad (1)$$

$$\text{Selectivity}(\%) = \frac{\text{Moles of certain product}}{\text{Moles of all oxidation products}} \times 100\% \quad (2)$$

The moles of alkyl peroxides were determined by the moles of triphenylphosphine oxide obtained through reduction of peroxides by triphenylphosphine at a molar ratio of 1 : 1. GC analyses were conducted on a Thermo Scientific Trace 1300 instrument with a flame ionization detector (FID), and the chromatographic column was a TG-5MS capillary column (30 m × 0.32 mm × 0.25 μm). HPLC analyses were conducted on a Thermo Scientific Ultimate 3000 instrument with an Ultimate 3000 photodiode array detector (PAD), and the chromatographic column was an Amethyst C_{18}–H chromatography column (150 mm × 4.6 mm × 0.25 μm). The mobile phase in HPLC analyses was a mixture of methanol and phosphoric acid aqueous solution (pH 2.2) in a volume ratio of 1 : 3, and the detection wavelength was 220 nm.

2.3. Quenching experiments

To investigate the mechanism of photocatalytic oxidation of C–H bonds with O_2 and determine the reactive species in detail, quenching experiments were carried out utilizing cyclohexane as a model substrate and tetrakis(4-carboxyphenyl)porphyrin (T(4-COOH)PP) as a representative photocatalyst in the presence of ethylenediaminetetraacetic acid disodium salt (EDTA-2Na) as a photogenerated hole (h^+) scavenger,[60,61] potassium persulfate ($K_2S_2O_8$) as a photogenerated electron (e^-) scavenger,[10,33,62] (2,2,6,6-tetramethylpiperidin-1-yl)oxyl (TEMPO) as a superoxide radical ion ($^{\bullet}O_2^-$) scavenger[27,30,63] or isopropanol (IPA) as a hydroxyl radical ($^{\bullet}OH$) scavenger.[12,34,64] In a glass reaction tube with a branch pipe and a high vacuum valve (25 mL), T(4-COOH)PP (4.0 mg, 5×10^{-3} mmol) and the quenching agent (2.5 mmol, 5%, mol mol^{-1}) were dispersed in cyclohexane(4.2080 g, 50 mmol), and the reaction tube was sealed with an oxygen balloon (1 atm). After stirring at 25 °C for 10 min, the reaction mixture was irradiated with a LED white light lamp (100 W) for 8.0 h. And the distance between the reaction tube and visible-light source was 4 cm. When the reaction was completed, triphenylphosphine (1.0492 g, 4 mmol) was added to the resultant reaction mixture with continued stirring for 15 min to transform the formed hydroperoxide. All the reaction mixture was transferred to a volumetric flask (25 mL), dissolved and made up to 25 mL exactly with acetone as the solvent. GC and HPLC analyses were carried out to calculate the conversion and selectivity following the procedure in 2.2.

2.4. EPR analysis

Electron paramagnetic resonance (EPR) analysis was conducted utilizing cyclohexane as a model substrate and T(4-COOH)PP as a representative photocatalyst in the presence of 5,5-dimethyl-1-pyrroline-*N*-oxide (DMPO) as a radical trapping agent.[19,20,27,33] In a glass reaction tube with a branch pipe and a high vacuum valve (25 mL), T(4-COOH)PP (4.0 mg, 5×10^{-3} mmol) was dispersed in cyclohexane (4.2080 g, 50 mmol), and the reaction tube was sealed with an oxygen balloon (1 atm). After stirring at 25 °C for 10 min, the reaction mixture was irradiated with a LED white light lamp (100 W) for 8.0 h. Then, 1 mL of the reaction mixture was taken out, and DMPO (1.1 mg, 0.01 mmol) was added to trap the free radical species for EPR measurements. The EPR measurement was conducted on a Bruker A300 instrument at room temperature. In the EPR analysis, the microwave frequency utilized was 9.85 GHz.

3. Results and discussion

3.1. Characterization and photoelectrochemical properties

The porphyrins and metalloporphyrins utilized as photocatalysts in this work were characterized and determined through ^{1}H NMR spectroscopy, ^{13}C NMR spectroscopy, ESI-MS and FT-IR spectroscopy, and the representative characterization spectra are presented in the SI.

As photocatalysts utilizing visible light as the energy source, the visible-light absorption properties of porphyrins and metalloporphyrins were investigated by UV-vis spectroscopy employing tetraphenylporphyrin (TPP), tetrakis(4-chlorophenyl)porphyrin (T(4-Cl)PP), tetrakis(4-methoxycarbonylphenyl)porphyrin (T(4-COOCH$_3$)PP), tetrakis(4-carboxyphenyl)porphyrin (T(4-COOH)PP), tetraphenylporphyrin cobalt(II) (TPP Co) and tetrakis(4-carboxyphenyl)porphyrin copper (II) (T(4-COOH)PP Cu) as typical model photocatalysts. It was illustrated obviously in Fig. 1(a) that all the model porphyrins and metalloporphyrins exhibited a strong absorption peak around 415 nm, which belonged to the Soret absorption band of porphyrins and metalloporphyrins.[65,66] And in the range of 500–650 nm, the four Q absorption bands of porphyrins and metalloporphyrins were observed too (Fig. 1(b)).[65,66] Both the Soret absorption band and Q absorption bands of porphyrins and metalloporphyrins were in the range of visible light, illustrating their strong absorption performance for visible light and their potential as photocatalysts under visible-light irradiation. The yield of photo-generated electrons and holes, as well as their recombination rates, are another important indicator of porphyrins and metalloporphyrins as photocatalysts. Thus, photoluminescence (PL) emission spectroscopy was utilized to characterize and predict the efficiency of porphyrins and metalloporphyrins in production of photo-generated electrons and holes and their recombination rates. In PL measurements, representative TPP, T(4-Cl)PP, T(4-COOCH$_3$)PP, T(4-COOH)PP, TPPCo, and T(4-COOH)PP Cu were employed as model photocatalysts. As demonstrated in Fig. 2, peripheral groups of porphyrins and metal centres exhibited a significant effect on their PL emission intensities, implying different recombination rates of photo-generated electrons and holes when porphyrins and metalloporphyrins were employed as photocatalysts. In general, the lower the PL emission intensities were, the slower the recombination rate was.[9,61] And the lower recombination rate of photo-generated electrons and holes is generally beneficial for improving the catalytic activity of photocatalysts. Hence, the diversity of porphyrin peripheral groups and metal centres would provide a huge catalyst library for porphyrin related

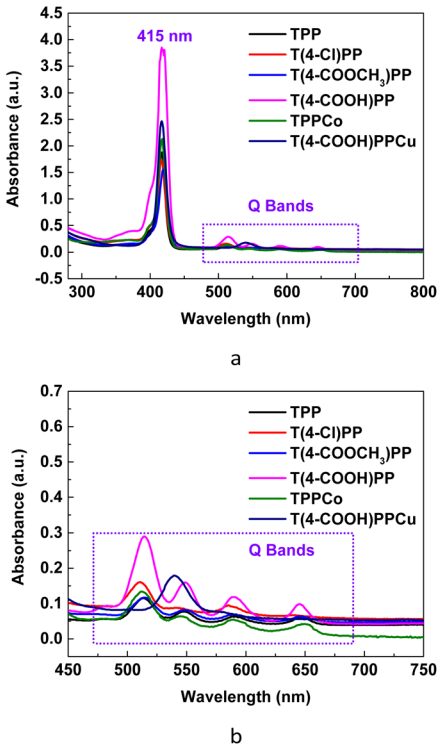

Fig. 1 UV-vis absorption spectra of representative porphyrins and metalloporphyrins in DMF (4×10^{-6} mol L^{-1}) (a) and their Q bands (b).

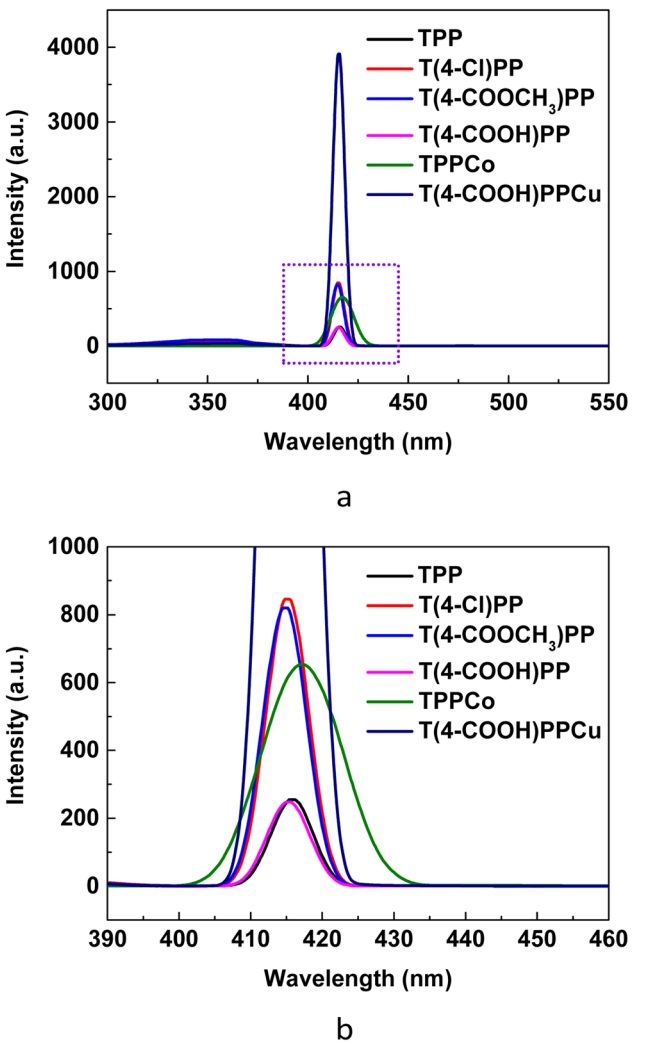

Fig. 2 PL emission spectra of representative porphyrins and metalloporphyrins in DMF (a), and local magnification (b) (4×10^{-6} mol L^{-1}).

photocatalytic reactions. In Fig. 2, lower PL emission intensities were observed when TPP and T(4-COOH)PP were selected as photocatalyst candidates, demonstrating great possibility and potential for application in photocatalytic oxidation in this work.

To further investigate the performance of porphyrins and metalloporphyrins in production of photo-generated electrons and holes and realization of the charge separation, transient photocurrent response was examined through intermittent light irradiation cycles utilizing representative TPP, T(4-Cl)PP, T(4-$COOCH_3$)PP, T(4-COOH)PP, TPP Co, and T(4-COOH)PP Cu as model photocatalysts. It is illustrated in Fig. 3(a) that an obvious transient photocurrent response could be observed when the selected porphyrins and metalloporphyrins were irradiated under visible light, indicating their superior performance in charge separation and production of photo-generated electrons. And for T(4-COOH)PP as a photocatalyst, the highest transient photocurrent density was obtained for selected photocatalysts, implying its potential as a better photocatalyst in this work, which was consistent with the prediction from the PL measurements. Moreover, it could also be obtained from Fig. 3(a) that, after five cycles of light-on and light-off irradiation, no decrease was observed in the transient photocurrent density, illustrating the stability and repeatability of selected porphyrins and metalloporphyrins as potential photocatalysts. The performance of porphyrins and metalloporphyrins in charge separation and migration was assessed through electrochemical impedance spectroscopy (EIS) as well. As shown in Fig. 3(b), in selected model photocatalysts, different arch radii were observed in the EIS Nyquist plots, illustrating their different impedance during charge migration. And T(4-COOH)PP and T(4-COOH)PP Cu exhibited smaller arch radii, indicating their smaller impedance to charge migration because of abundant protonic hydrogens (H^+) in their structures,[20,24] based on which T(4-COOH)PP and T(4-COOH)PP Cu were speculated to have better photocatalytic activity following oxidation of C–H bonds with O_2 irradiated under visible light. The results of EIS measurements were in good agreement with the PL test and transient photocurrent test.

Based on the characterization studies and measurements above, it could be concluded that as the chemical models of chlorophyll, porphyrins and metalloporphyrins possessed strong absorption performance for visible light, and abundant photo-generated electrons and holes could be produced through charge separation under irradiation of visible light. In particular, for tetrakis(4-carboxyphenyl)porphyrin (T(4-COOH)PP) as the potential photocatalyst, strong visible-light absorption, lower recombination rates of photo-generated electrons and holes, higher transient photocurrent density and smaller impedance to charge migration were achieved simultaneously. Thus, it could be predicted that T(4-COOH)PP is a good choice to act as a photocatalyst in this work.

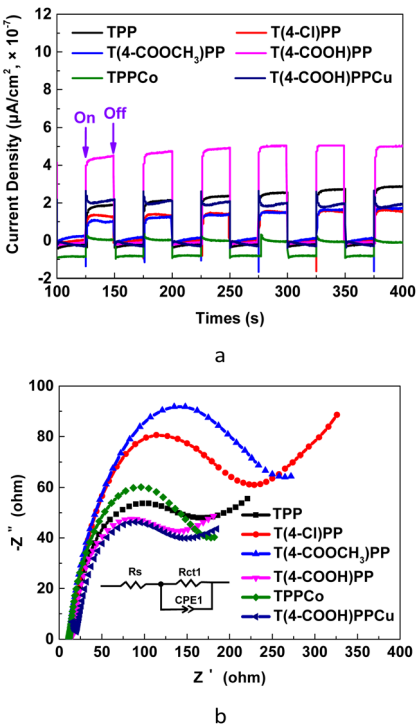

Fig. 3 Transient photocurrent spectroscopy (a) and electrochemical impedance spectroscopy (EIS) (b) of representative porphyrins and metalloporphyrins.

3.2. Photocatalytic oxidation performance

3.2.1. Preliminary exploration experiments. To realize the insertion of oxygen element into C–H bonds through a greener and sustainable chemical process with lower energy consumption and lower carbon emissions, the feasibility of photocatalytic oxidation of C–H bonds with O_2 irradiated under visible light employing porphyrins as photocatalysts was investigated at first. The necessity of visible light, porphyrins and O_2 in oxidation of C–H bonds was explored systematically utilizing the important cyclohexane oxidation in the chemical industry as a model reaction. As demonstrated in Table 1, no conversion of cyclohexane was observed under the conditions of no visible light, no catalyst and no O_2 (Entry 1 in Table 1), and in the presence of only visible light, porphyrin catalyst or O_2, the conversion of cyclohexane was still at a negligible level (<0.05 mmol ($g_{cat.}^{-1}$ h^{-1})) (Entries 2–5 in Table 1), indicating that (1) just irradiation under visible-light, C–H bonds could not be transformed to their oxidation products without catalyst and O_2 (Entry 2 in Table 1), (2) both cyclohexane and porphyrin catalysts could not be converted into oxidation products of C–H bonds spontaneously without O_2 (Entries 3 and 4 in Table 1), and (3) C–H bonds could not be oxidized by O_2 without catalyst and light under the conditions in this work (Entry 5 in Table 1). From the experimental data (Entries 6 and 7 in Table 1), it could be found that in the absence of O_2, not only C–H bonds could not be converted to their oxidation products under the conditions of visible-light irradiation in the presence of photocatalysts but also catalysts (TPP and T(4-Br)PP) could not be converted to oxidation products too, demonstrating the stability of porphyrins as photocatalysts. And in the presence of O_2, visible light exhibited some catalytic performance without

Table 1 Feasibility study in the photocatalytic oxidation of C–H bonds with O_2[a]

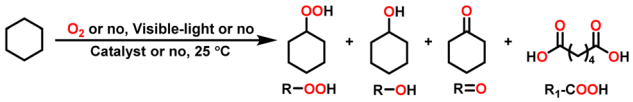

Entry	Reaction conditions	Conversion (mmol ($g_{cat.}^{-1}$ h^{-1}))	Selectivity (%)	
			R–OOH	R=O
1	No light, no catalyst, and no O_2	—	—	—
2	Light, no catalyst, and no O_2	<0.05	—	—
3[b]	No light, catalyst, and no O_2	<0.05	—	—
4[c]	No light, catalyst, and no O_2	<0.05	—	—
5	No light, no catalyst, and O_2	<0.05	—	—
6[b]	Light, catalyst, and no O_2	<0.05	—	—
7[c]	Light, catalyst, and no O_2	<0.05	—	—
8	Light, no catalyst, and O_2	0.13	69.2	30.8
9[b]	No light, catalyst, and O_2	<0.05	—	—
10[c]	No light, catalyst, and O_2	<0.05	—	—
11[b]	Light, catalyst, and O_2	3.03	99.9	0.1
12[c]	Light, catalyst, and O_2	2.69	99.3	0.7

[a] Reaction conditions: cyclohexane (4.2080 g, 50 mmol), LED white light lamp (100 W), stirring speed (600 rpm), room temperature (25 °C), and reaction time (8.0 h). [b] Tetraphenylporphyrin (TPP) as a catalyst (5×10^{-3} mmol, 3.1 mg, 0.01%, mol mol^{-1}). [c] Tetrakis(4-bromophenyl) porphyrin (T(4-Br)PP) as a catalyst (5×10^{-3} mmol, 4.7 mg, 0.01%, mol mol^{-1}).

photocatalyst. In the oxidation of cyclohexane with O_2 irradiated with visible light in the absence of photocatalyst, the conversion reached up to 0.13 mmol ($g_{cat.}^{-1}$ h^{-1}) (Entry 8 in Table 1), which still was at a very low level. But no catalytic ability was observed from porphyrins (TPP and T(4-Br)PP) in the oxidation of C–H bonds with O_2 in the absence of visible light under the conditions of this work (Entries 9 and 10 in Table 1), illustrating the necessity of light in this work. Only when visible light, porphyrin catalysts and O_2 were presented simultaneously, obvious oxidation of C–H bonds occurred. In the oxidation of cyclohexane with O_2 utilizing TPP and T(4-Br)PP as photocatalysts under irradiation of visible light, the conversion reached up to 3.03 mmol ($g_{cat.}^{-1}$ h^{-1}) and 2.69 mmol ($g_{cat.}^{-1}$ h^{-1}), respectively, with the selectivity of more than 99% to cyclohexyl hydroperoxide, which was the important intermediate product in cyclohexane oxidation and could be transformed to cyclohexanol and cyclohexanone (KA oil) smoothly. From the exploration experiments above, not only it could be concluded that it was feasible to insert oxygen atoms into C–H bonds with O_2 as the oxidant irradiated under visible-light employing porphyrins as photocatalysts but also it was confirmed that all the visible light, porphyrin catalysts and O_2 were indispensable in this oxidation process.

3.2.2. Effect of photocatalyst structure. With confirmation on the feasibility to conduct photocatalytic oxidation of C–H bonds with O_2 irradiated under visible light employing porphyrins as photocatalysts, the effect of porphyrin structure on oxidation of C–H bonds was explored in detail as the key factor. As illustrated in Table 2 and Fig. 4, in the employment of cyclohexane oxidation as a model reaction, all the porphyrins with different peripheral groups (electron-withdrawing or -donating) and different electronic environments, the corresponding metalloporphyrins possessed the capability to act as photocatalysts in oxidation of C–H bonds with O_2 irradiated under visible light. A conversion range from 2.49 mmol ($g_{cat.}^{-1}$ h^{-1}) to 3.18 mmol ($g_{cat.}^{-1}$ h^{-1}) was obtained with the selectivity of more than 99% to cyclohexyl hydroperoxide ($C_6H_{11}OOH$). In particular, for tetrakis(4-carboxyphenyl) porphyrin (T(4-COOH)PP) as the photocatalyst, the substrate conversion reached up to 3.18 mmol ($g_{cat.}^{-1}$ h^{-1}) with a selectivity of 99.9% to cyclohexyl hydroperoxide (Entry 20 in Table 2). It was also observed from Fig. 4 that no positive impact was generated from the formation of metalloporphyrins. Thus, in this work, tetrakis(4-carboxyphenyl)porphyrin (T(4-COOH)PP) was regarded as the preferred photocatalyst to conduct the following experiments for its convenient synthesis. In the utilization of T(4-COOH)PP as the photocatalyst, not only the highest catalytic performance among the selected chemical models of chlorophyll (porphyrins and metalloporphyrins) in this work was obtained but also higher conversion and selectivity than the derivative of natural chlorophyll (chlorophyllin) were achieved. As shown in Table 2, the conversion of cyclohexane was 2.68 mmol ($g_{cat.}^{-1}$ h^{-1}) with a selectivity of 99.8% towards cyclohexyl hydroperoxide (Entry 21 in Table 2) in the utilization of chlorophyllin as the photocatalyst. Then, the source of better catalytic performance exhibited by T(4-COOH)PP was explored in depth by means of photoluminescence (PL) emission spectroscopy, time-resolved photoluminescence (TRPL) spectroscopy, transient photocurrent spectroscopy and electrochemical impedance spectroscopy (EIS).

In the photoluminescence (PL) emission spectra of representative porphyrins (Fig. 5(a)), TPP and T(4-COOH)PP exhibited lower PL emission intensities, implying their lower recombination rate of photo-generated electrons and holes,

Table 2 Effect of porphyrins on photocatalytic oxidation of C–H bonds with O_2[a]

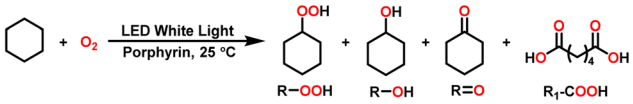

Entry	Porphyrins[b]	Conversion (mmol ($g_{cat.}^{-1}$ h^{-1}))	Selectivity (%)	
			R–OOH	R= O
1	TPP	3.03	99.9	0.1
2	T(2-Cl)PP	2.62	99.8	0.2
3	T(3-Cl)PP	2.65	99.7	0.3
4	T(4-Cl)PP	2.76	99.7	0.3
5	T(4-Br)PP	2.69	99.3	0.7
6	T(4-F)PP	2.87	99.7	0.3
7	T(4-CN)PP	2.81	99.8	0.2
8	T(4-CF_3)PP	2.92	99.9	0.1
9	T(2,4,6-triCl)PP	2.54	99.1	0.9
10	T(2,3,6-triF)PP	2.49	99.8	0.2
11	T(2,4,6-triF)PP	2.78	99.2	0.8
12	T(2,3,4,5,6-pentaF)PP	2.59	99.2	0.8
13	T(2-CH_3)PP	2.78	99.8	0.2
14	T(3-CH_3)PP	2.76	99.8	0.2
15	T(4-CH_3)PP	2.58	99.3	0.7
16	T(2-OCH_3)PP	2.94	99.8	0.2
17	T(3-OCH_3)PP	2.86	99.8	0.2
18	T(4-OCH_3)PP	2.62	99.5	0.5
19	T(4-$COOCH_3$)PP	2.77	99.6	0.4
20	T(4-COOH)PP	3.18	99.9	0.1
21	Chlorophyllin	2.68	99.8	0.2

[a] Reaction conditions: cyclohexane (4.2080 g, 50 mmol), porphyrin catalyst (5×10^{-3} mmol, 0.01%, mol mol^{-1}), LED white light lamp (100 W), stirring speed (600 rpm), room temperature (25 °C), and reaction time (8.0 h). [b] Porphyrin abbreviation: for example, T(2,4,6-triCl)PP is the abbreviation of tetrakis(2,4,6-trichlorophenyl)porphyrin. T is the abbreviation of tetrakis, 2,4,6-triCl is the abbreviation of the position and number of substituents on phenyl, the first P is the abbreviation of phenyl, and the second P is the abbreviation of porphyrin.

which was consistent with their higher photocatalytic activity, as shown in Table 2 (Entry 1 and Entry 20). When photocatalysts were converted from TPP and T(4-COOH)PP to T(4-Cl)PP and T(4-$COOCH_3$)PP, the PL emission intensities increased. as demonstrated in Fig. 5(a), and the substrate conversion in oxidation of cyclohexane decreased from 3.03 mmol ($g_{cat.}^{-1}$ h^{-1}) and 3.18 mmol ($g_{cat.}^{-1}$ h^{-1}) to 2.76 mmol ($g_{cat.}^{-1}$ h^{-1}) and 2.77 mmol ($g_{cat.}^{-1}$ h^{-1}) (Entry 4 and Entry 19 in Table 2) as a result of faster recombination rate of photo-generated electrons and holes. And in Fig. 5(a), T(4-Br)PP and TPFPP possessed the highest PL emission intensities along with their lowest substrate conversion (2.69 mmol ($g_{cat.}^{-1}$ h^{-1}) and 2.59 mmol ($g_{cat.}^{-1}$ h^{-1})) among the selected representative porphyrins (Entry 5 and Entry 12 in Table 2). A similar profile between substrate conversion and PL emission intensity was also observed in the utilization of metalloporphyrins as photocatalysts (Fig. 5(b)). Thus, the recombination rate of photo-generated electrons and holes was regarded as the first important influencing factor in photocatalytic oxidation of C–H bonds with O_2 irradiated under visible light in this work. The lower the recombination rate of photo-generated electrons and holes was, the higher the catalytic activity of photocatalysts was. The recombination rate of photo-generated electrons and holes was further investigated through time-resolved photoluminescence (TRPL) spectroscopy. As shown in Fig. 5(c), the longest photo-generated electron lifetime was obtained in the utilization of T(4-COOH)PP as a photocatalyst, and the lifetime of photo-generated electrons reached up to 5.03 ns, which conformed with the results of PL emission spectra (Fig. 5(a and b)) and the higher catalytic performance of T(4-COOH)PP exhibited in Table 2 (Entry 20).

To further probe the source of porphyrins and metalloporphyrins as photocatalysts, their performance in charge separation and production of photo-generated electrons was investigated through the measurement of transient photocurrent responses. As shown inFig. 5(d and e), the highest transient photocurrent density was obtained when T(4-COOH)PP was selected as the photocatalyst among all the representative porphyrins and metalloporphyrins, implying its superior function in inducing charge separation and production of photo-generated electrons under irradiation of visible light. The characterization results of transient photocurrent response were in good agreement with the superior catalytic performance of T(4-COOH)PP exhibited in Table 2 (Entry 20), which also confirmed the characterization results in PL emission spectra and TRPL spectra. Thus, the superior performance of T(4-

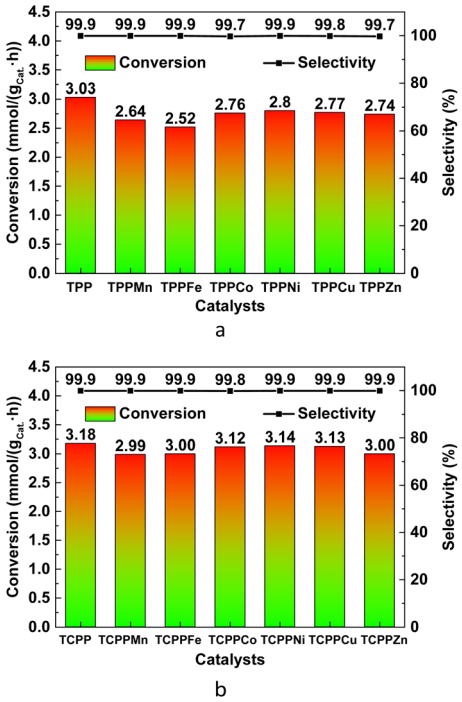

Fig. 4 Effect of metal centres on photocatalytic oxidation of C–H bonds with O_2 using TPP as ligand (a) and TCPP as ligand (b). Reaction conditions: cyclohexane (4.2080 g, 50 mmol), porphyrin catalyst (5×10^{-3} mmol, 0.01%, mol mol^{-1}), LED white light lamp (100 W), stirring speed (600 rpm), room temperature (25 °C), and reaction time (8.0 h). TCPP is the abbreviation of tetrakis(4-carboxyphenyl)porphyrin (T(4-COOH)PP).

COOH)PP in inducing charge separation was regarded as its second beneficial influencing factor in photocatalytic oxidation of C–H bonds with O_2. In the electrochemical impedance spectroscopy (EIS), as shown in Fig. 5(f) and S46, the smaller arch radius was observed from the EIS Nyquist plots of T(4-COOH)PP, illustrating its lower impedance during charge migration, which was the third important promoting factor for photocatalytic reactions. All the photoelectrochemical characterization experiments and measurements exhibited good agreement with the superior photocatalytic performance of T(4-COOH)PP in oxidation of C–H bonds with O_2 irradiated under visible light.

Therefore, based on the systematic study on photocatalytic performance and photoelectrochemical characterization studies above, all the selected porphyrins and metalloporphyrins possessed the capability to catalyze the oxidation of C–H bonds with O_2 under irradiation of visible light, and tetrakis(4-carboxyphenyl)porphyrin (T(4-COOH)PP) exhibited superior photocatalytic performance than others, in which the substrate conversion reached up to 3.18 mmol ($g_{cat.}^{-1}$ h^{-1}) with a selectivity of 99.9% to cyclohexyl hydroperoxide in cyclohexane oxidation. The satisfying catalytic capability of T(4-COOH)PP was mainly attributed to its higher visible-light absorption, charge separation, production of photo-generated electrons and lower impedance during charge migration under irradiation of visible light, as illustrated in Fig. 1 and 5.

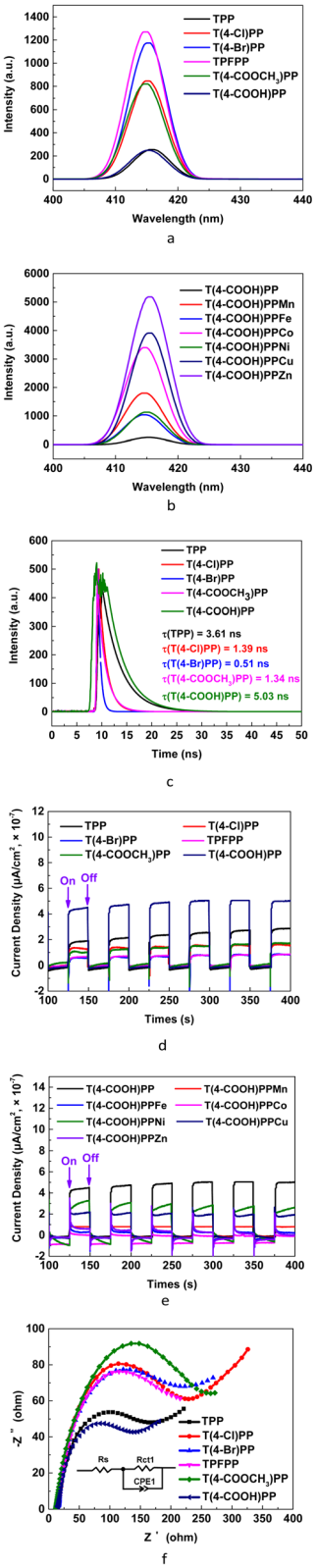

Fig. 5 PL emission spectra ((a and b), 4×10^{-6} mol L^{-1}), time-resolved photoluminescence (TRPL) spectra (c), transient photocurrent spectroscopy (d and e) and electrochemical impedance spectroscopy (EIS) (f) of representative porphyrins and metalloporphyrins.

The photocatalytic performance and photoelectrochemical characterization exhibited good consistency.

3.2.3. Further optimization and catalyst stability. With the determination of the optimized photocatalyst, the oxidation of C–H bonds using O_2 catalyzed by T(4-COOH)PP under irradiation of visible light was further optimized from the aspects of light intensity, catalyst amount and reaction time. And the stability of T(4-COOH)PP in photocatalytic oxidation of C–H bonds was also evaluated through cycle experiments utilizing cyclohexane oxidation as the model reaction. As illustrated in Fig. 6(a), the substrate conversion exhibited an upward trend with the increase of light intensity, and the selectivity towards oxidation product maintained above 99%. Striking a balance between catalytic efficiency and energy consumption, the light intensity was selected as 100 W in this work, in which the substrate conversion reached up to 3.18 mmol ($g_{cat.}^{-1}$ h^{-1}) with the selectivity of 99.9%. As for the effect of catalyst amount (Fig. 6(b)), due to the aggregation of catalysts and the unit of conversion being mmol ($g_{cat.}^{-1}$ h^{-1}), a decreasing trend was observed from the profile between substrate conversion and catalyst amount. Hence, the catalyst amount in this work was selected as 0.01% (mmol $mmol^{-1}$). It was demonstrated in Fig. 6(c) that the generation rate of oxidation products decreased along with the increased reaction time, and in the first hour, substrate conversion reached up to 22.38 mmol ($g_{cat.}^{-1}$ h^{-1}) with a selectivity of 99.9%. The decreased generation rate of oxidation products was mainly attributed to the consumption of O_2 adsorbed from air by the catalyst, and in the later stage of reaction, O_2 at atmospheric pressure diffused into the reaction system in a relatively low rate. When T(4-COOH)PP was kept under a N_2 atmosphere for 24.0 h to replace adsorbed O_2, the substrate conversion decreased from 22.38 mmol ($g_{cat.}^{-1}$ h^{-1}) to 10.86 mmol ($g_{cat.}^{-1}$ h^{-1}) in the first hour of the reaction, which confirmed our speculation. Because of the insolubility of T(4-COOH)PP in cyclohexane, its stability and reusability in photocatalytic oxidation of C–H bonds with O_2 was evaluated through cycle experiments. After each experiment, T(4-COOH)PP was filtered, washed with cyclohexane, dried, and subjected to cycle experiments. As shown in Fig. 6(d), in five consecutive experiments, the substrate conversion of cyclohexane oxidation was maintained above 2.70 mmol ($g_{cat.}^{-1}$ h^{-1}) with a selectivity higher than 99% towards cyclohexyl hydroperoxide, implying the stability and reusability of T(4-COOH)PP in photocatalytic oxidation of C–H bonds with O_2.

Thus, based on the systematic optimization and cycle experiments, a sustainable, low-energy consumption and feasible C–H bond oxidation strategy has been developed under mild conditions in this work. In this procedure, tetrakis(4-carboxyphenyl)porphyrin (T(4-COOH)PP) was utilized as a photocatalyst, and visible light from an LED white light lamp (100 W) was employed as the energy source. Under solvent-free conditions and room temperature, the substrate conversion reached up to 3.18 mmol ($g_{cat.}^{-1}$ h^{-1}) with the selectivity of 99.9% to alkyl hydroperoxide within the reaction time of 8.0 h utilizing cyclohexane oxidation as the model reaction.

3.2.4. Substrate scope and literature comparison. With the confirmation on the feasibility and correctness of C–H bond oxidation with O_2 under irradiation of visible light and utilizing T(4-COOH)PP as the photocatalyst, the substrate scope was extended to other cycloalkanes and alkyl aromatics possessing

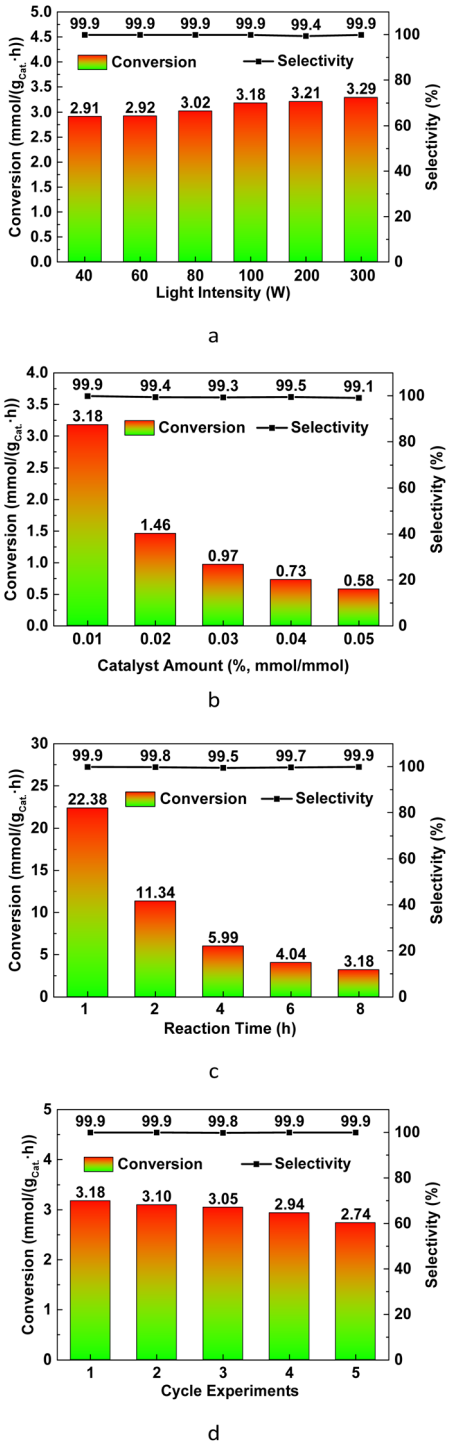

Fig. 6 Effect of light intensity (a), catalyst amount (b), and reaction time (c) on photocatalytic oxidation of C–H bonds with O_2, and cycle experiments (d). Reaction conditions: cyclohexane (4.2080 g, 50 mmol), T(4-COOH)PP as the catalyst (mol mol^{-1}), LED white light lamp (100 W or others), stirring speed (600 rpm), room temperature (25 °C), and reaction time (8.0 h or others).

Table 3 Substrate scope of C–H bond oxidation with O_2 irradiated under visible light and catalyzed by T(4-COOH)PP[a]

Entry	Substrates	Products	Conversion (mmol ($g_{cat.}^{-1}$ h^{-1}))	Selectivity (%)
1		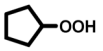	3.12	99.9
2		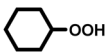	3.18	99.9
3		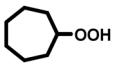	3.25	99.5
4		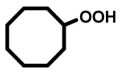	3.42	99.7
5	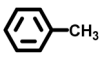	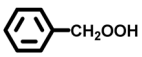	3.10	99.3
6	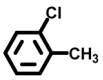	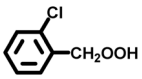	2.85	99.9
7	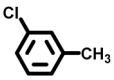	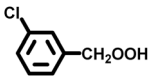	2.79	99.9
8	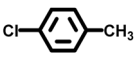	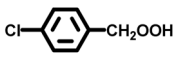	3.21	99.8
9	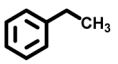	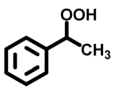	3.92	98.4
10	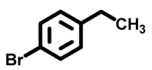	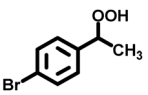	3.95	99.9
11	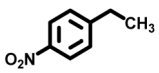	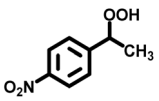	3.61	99.9
12		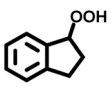	3.73	97.8
13		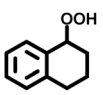	2.63	99.9
14	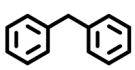	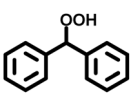	2.95	99.3
15	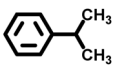	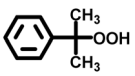	4.02	99.9
16	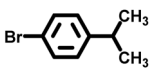	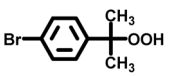	4.00	99.9
17	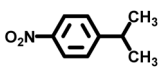	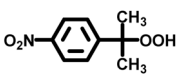	4.06	97.5
18	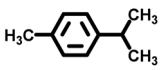	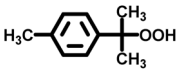	3.89	97.2

[a] Reaction conditions: substrate (50 mmol), T(4-COOH)PP (4.0 mg, 5×10^{-3} mmol, 0.01%, mol mol^{-1}), LED white light lamp (100 W), stirring speed (600 rpm), room temperature (25 °C), and reaction time (8.0 h).

α-C–H bonds. As demonstrated in Table 3, all the typical C–H bonds in cycloalkanes and alkyl aromatics could be transformed to their corresponding alkyl hydroperoxides under irradiation of visible light in the utilization of O_2 as an oxidant and simple porphyrin T(4-COOH)PP as a photocatalyst, realizing the insertion of oxygen element into C–H bonds. A substrate conversion range from 2.63 mmol ($g_{cat.}^{-1}$ h^{-1}) to 4.06 mmol ($g_{cat.}^{-1}$ h^{-1}) was obtained under the conditions of low energy consumption and lower carbon emissions, and the selectivity to main products alkyl hydroperoxides reached up to 97–99%, which not only could be employed as an industrial oxidant but also could be conveniently converted into other chemical products. Therefore, the method developed in this work for C–H bonds' photocatalytic oxidation is of great significance for the low-energy consumption, green and sustainable conversion and utilization of hydrocarbons, as well as for the syntheses of other oxygen-containing chemical products and intermediates. It was also found from the study on substrate scope, the substrate conversion exhibited a high correlation with the dissociation energy of C–H bonds in cycloalkanes and α-C–H bonds in alkyl aromatics. As demonstrated in Fig. 7, the correlation between substrate conversion and dissociation energy of C–H bonds reached up to 0.9823 and 0.9888, respectively, in the oxidation of cycloalkanes and alkyl aromatics, implying that the dissociation of C–H bonds is the key step in the insertion of oxygen element into C–H bonds in this work.

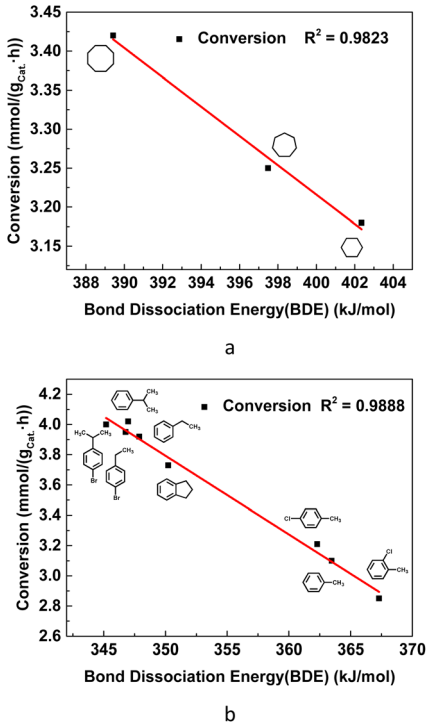

Fig. 7 The correlation between substrate conversion and bond dissociation energy of C–H bonds in cycloalkanes (a) and α-C–H bonds in alkyl aromatics (b). The bond dissociation energy (BDE) was obtained through quantum chemical calculations utilizing the Gaussian 16 program.[67] All the substrate molecules and radicals were optimized at the level of B3LYP/def2SVP first, and then the bond dissociation energy (BDE) was calculated through the following equation, $BDE_{R-H} = H_{R\cdot} + H_{H\cdot} - H_{R-H}$.

Then, the strategy developed in this work was compared with methods reported in the literature for photocatalytic oxidation of C–H bonds utilizing the important cyclohexane oxidation in the chemical industry as a comparative model. Representative examples irradiated under visible light and conducted at room temperature with reasonable experimental data are presented in Table 4. At the present stage, the production efficiency of oxidation products in the important cyclohexane oxidation with O_2 irradiated under visible light at room temperature is usually at the level of μmol ($g_{cat.}^{-1}$ h^{-1}), and in some examples volatile and toxic organic solvents were employed. However, through learning from nature and utilizing the chemical model of chlorophyll and tetrakis(4-carboxyphenyl)porphyrin (T(4-COOH)PP) as the photocatalyst, not only the solvent-free oxidation of C–H bonds with O_2 under irradiation of visible light at room temperature was achieved in this work but also the generation efficiency of oxidation products in the utilization of cyclohexane oxidation as a model reaction reached up to 3.18 mmol ($g_{cat.}^{-1}$ h^{-1}) with a selectivity of 99% towards cyclohexyl hydroperoxide, which could be transformed to cyclohexanol and cyclohexanone (KA oil) smoothly. Compared with current literature, the main advantages of the oxidation method developed in this work are high efficiency in insertion of oxygen element into C–H bonds, high selectivity towards alkyl hydroperoxides and mild conditions. And as photocatalysis utilizing visible light as the energy source, the strategy developed in this work is also a low-energy consumption, low-emission and sustainable route for C–H bond oxidation. Therefore, based on the investigation into substrate scope and literature comparison, this work not only was an efficient and sustainable approach to insert oxygen element into C–H bonds under mild conditions but also could be employed as a low-energy consumption, low-emission and sustainable route to transform and utilize abundant hydrocarbons in the chemical industry.

3.3. Possible catalytic mechanism

To further understand the process of C–H bond oxidation with O_2 under irradiation of visible light and in the presence of tetrakis(4-carboxyphenyl)porphyrin (T(4-COOH)PP) as a photocatalyst, the oxidation mechanism in this work was investigated in detail. To verify the reactive species in photocatalytic oxidation of C–H bonds with O_2, quenching experiments were carried out utilizing cyclohexane as a model substrate and tetrakis(4-carboxyphenyl)porphyrin (T(4-COOH)PP) as a photocatalyst. In quenching experiments, ethylenediaminetetraacetic acid disodium salt (EDTA-2Na) was utilized as a photogenerated hole (h^+) scavenger,[60,61] potassium persulfate ($K_2S_2O_8$) as a photogenerated electron (e^-) scavenger,[10,33,62] (2,2,6,6-tetramethylpiperidin-1-yl)oxyl (TEMPO) as a superoxide radical ion ($^{\cdot}O_2^-$) scavenger[27,30,63] and isopropanol (IPA) as a hydroxyl radical ($^{\cdot}OH$) scavenger.[12,34,64] As demonstrated in Fig. 8(a), the conversion decreased drastically from 3.18 mmol ($g_{cat.}^{-1}$ h^{-1}) to

Table 4 Representative photocatalytic oxidation of cyclohexane irradiated under visible light at room temperature

Entry	Reaction conditions	Conversion (mmol ($g_{cat.}^{-1}$ h^{-1}))	Selectivity[a] (%)	References
1	Nitrogen-doped and carbon-modified TiO_2 as a catalyst, 1 atm O_2, 25 °C, 300 W Xe lamp, and CCl_4 as a solvent	0.72	>99	25
2	Nitrogen-doped mixed-phase TiO_2 as a catalyst, 1 atm O_2, 25 °C, 300 W Xe lamp, and CCl_4 as a solvent	0.45	>99	32
3	Nitrogen-doped TiO_2 as a catalyst, 1 atm O_2, 25 °C, $\lambda \geq 420$ nm visible light, and CCl_4 as a solvent	0.83	>99	27
4	Thiophene-based covalent triazine polymer as a catalyst, 1 atm O_2, 25 °C, 10 W blue LED lamp, and 2.0 M HCl aqueous solution as a solvent	0.61	>99	64
5	$Mg_3Al_{0.5}Cr_{0.5}O_{4.5}$/N-doped TiO_2 as a catalyst, 1 atm O_2, 25 °C, $\lambda \geq 400$ nm visible light, and acetonitrile as a solvent	7.05	>99	68
6	WO_3/C_3N_4 as a catalyst, 1 atm O_2, 15 °C, 300 W Xe lamp, and H_2O as a solvent	0.14	>99	29
7	Ultrathin Bi_2WO_6/BiOCl nanosheets as a catalyst, 1 atm air, 20 °C, 500 W Hg lamp, and solvent-free	1.05	>99	35
8	Defect-rich nitrogen-doped Nb_2O_5 as a catalyst, 1 atm O_2, 25 °C, 300 W Xe lamp, and solvent-free	0.24	>99	31
9	Nb_2O_5 nanoparticles on BiOCl nanosheets as a catalyst, 1 atm O_2, 25 °C, 300 W Xe lamp, and solvent-free	0.31	>99	20
10	$Cs_3Bi_2Br_9$ perovskite nanocrystals on 2D $Ti_3C_2T_x$ MXene as a catalyst, 1 atm O_2, 20 °C, 5 W blue LED lamp, and solvent-free	0.49	>99	69
11	Vacancy-ordered methylammonium tin bromide as ca atalyst, 1 atm O_2, 25 °C, simulated visible light: 100 mW cm^{-2}, and solvent-free	0.026	>99	30
12	Hexagonal boron nitride/TiO_2 as a catalyst, 1 atm O_2, 25 °C, λ >300 nm visible light, and solvent-free	0.076	85.4	70
13	Hierarchical BiOCl as a catalyst, 1 atm air, 20 °C, 500 W Hg lamp, and solvent-free	0.99	>99	28
14	T(4-COOH)PP as a catalyst, 1 atm O_2, 25 °C, 100 W white LED lamp, and solvent-free	3.18	> 99	This work

[a] Total selectivity to partial oxidation products such as cyclohexanol, cyclohexanone, and cyclohexyl hydroperoxide.

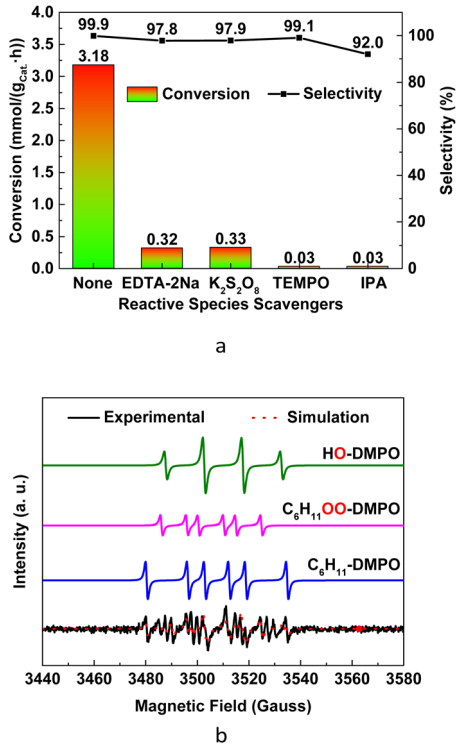

Fig. 8 Quenching experiments (a) and EPR measurements (b) of cyclohexane oxidation with O_2 irradiated under visible light utilizing T(4-COOH)PP as the photocatalyst.

0.32 mmol ($g_{cat.}^{-1}$ h^{-1}), 0.33 mmol ($g_{cat.}^{-1}$ h^{-1}), 0.03 mmol ($g_{cat.}^{-1}$ h^{-1}) and 0.03 mmol ($g_{cat.}^{-1}$ h^{-1}), respectively, in the utilization of EDTA-2Na, $K_2S_2O_8$, TEMPO and IPA as reactive species scavengers, respectively, in 5% of substrate moles, implying that all the four reactive species existed in the model reaction and played indispensable roles. The reactive species in photocatalytic oxidation of C–H bonds in this work were also investigated utilizing EPR measurements. From the EPR spectra (Fig. 8(b)), it could be observed that in the model reaction of cyclohexane oxidation, the main reactive species contained cycloalkyl carbon centred free radicals ($C_6H_{11}^{\bullet}$), cycloalkyl peroxide radicals ($C_6H_{11}OO^{\bullet}$) and hydroxyl radicals ($HO^{\bullet}$), implying the free radical mechanism of this work. Therefore, the reactive species involved in the photocatalytic oxidation of C–H bonds in this work included photogenerated electrons (e^-), corresponding holes (h^+), superoxide radical ions ($^{\bullet}O_2^-$), hydroxyl radicals ($^{\bullet}OH$), alkyl carbon centred free radicals ($C_6H_{11}^{\bullet}$) and alkyl peroxide radicals ($C_6H_{11}OO^{\bullet}$), which provided a solid foundation for the following mechanism research.

As an insoluble and clustered solid photocatalyst, the band-gap energy (E_g), valence band (VB) position and conduction band (CB) position of T(4-COOH)PP were investigated in the mechanism study as well. The E_g value of T(4-COOH)PP was obtained through derivatizing its UV-vis absorption spectrum (Fig. 9(a)) and getting the extremum (X, k) in the first derivative curve of UV-vis absorption (Fig. 9(b)). Then a line with a slope of k was drawn at the extremum point (X, Y) of absorption curve. The intersection of this line with the X-axis was the threshold of

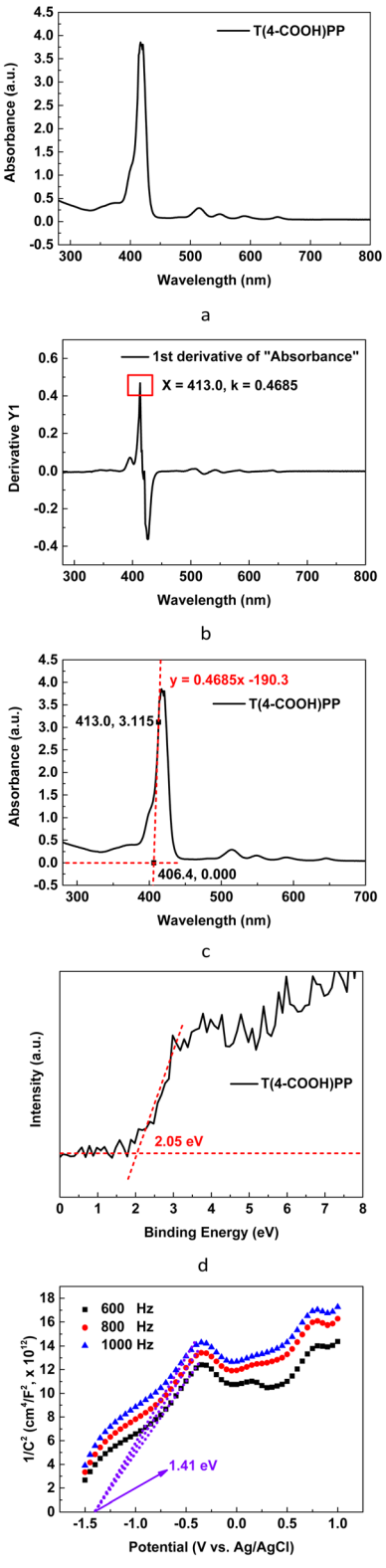

Fig. 9 UV-vis absorption spectrum of T(4-COOH)PP (a) and its derivatives (b and c), XPS valence band of T(4-COOH)PP (d), and Mott–Schottky curves of T(4-COOH)PP (e).

absorption wavelength (λ_g) (Fig. 9(c)), and E_g was calculated following the equation $E_g = 1240/\lambda_g = 1240/406.4 = 3.05$ eV. The valence band (VB) position was obtained through valence band XPS of T(4-COOH)PP. As shown in Fig. 9(d), the valence-band potential ($E_{VB,\ XPS}$) of T(4-COOH)PP relative to the Fermi energy level was 2.05 eV. Thus, the valence-band potential ($E_{VB,\ NHE}$) of T(4-COOH)PP relative to the standard hydrogen electrode could be calculated following $E_{VB,\ NHE} = \varphi + E_{VB,\ XPS} - 4.44$, where φ is an operating parameter of the XPS instrument[33,71] and 4.20 eV in this work. Consequently, the $E_{VB,\ NHE}$ of T(4-COOH)PP was obtained as 1.81 eV. As for the conduction band (CB) position of T(4-COOH)PP, it was calculated through the equation $E_{CB} = E_{VB} - E_g = 1.81 - 3.05 = -1.24$ eV. The conduction band (CB) position was also verified through the Mott–Schottky plots of T(4-COOH)PP at frequencies of 600, 800 and 1000 Hz, as shown in Fig. 9(e). The flat-band potential (E_{fb}) of T(4-COOH)PP relative to the Ag/AgCl electrode was obtained through determining the intersection of linear parts in Mott–Schottky curves with the *X*-axis and acquired as −1.41 eV. Thus the flat-band potential (E_{fb}) of T(4-COOH)PP relative to the standard hydrogen electrode was calculated following the equation $E_{fb,\ NHE} = E_{fb,\ Ag/AgCl} + 0.197 = -1.41 + 0.197 = -1.213$ eV.[33,71] As an n-type semiconductor, because the $E_{fb,\ NHE}$ is approximately 0.2 eV higher than its conduction band (CB) position, the E_{CB} was calculated through $E_{CB} = E_{fb,\ NHE} - 0.2 = -1.413$ eV.[27,72] The E_{CB} value obtained based on Mott–Schottky plots (−1.413 eV) exhibited excellent consistency with the value calculated through the equation $E_{CB} = E_{VB} - E_g$ (−1.24 eV), implying the rationality and accuracy of the band gap energy (E_g), valence band position (E_{VB}) and conduction band position (E_{CB}) obtained in this work.

Based on the exploratory research above and related references,[9,12,20,27,73] the reaction mechanism in photocatalytic oxidation of C–H bonds with O_2 under irradiation of visible light utilizing tetrakis(4-carboxyphenyl)porphyrin (T(4-COOH)PP) as a photocatalyst was speculated and demonstrated in Fig. 10, in which cyclohexane was utilized as a model substrate. At first, under irradiation of visible light, electrons in the VB were excited and transferred to the CB, generating the photo-generated electrons (e^-) and holes (h^+). Then, in the VB, cyclohexane (C_6H_{12}) was oxidized by holes (h^+) to the cyclohexyl radical ($C_6H_{11}^{\bullet}$) and hydrogen cation (H^+), and the obtained $C_6H_{11}^{\bullet}$ was transformed to the cycloalkyl peroxide radical ($C_6H_{11}OO^{\bullet}$) through capturing molecular oxygen (O_2). Oxidation products cyclohexyl hydroperoxides were produced through abstraction of a hydrogen atom from cyclohexane with the generation of the cyclohexyl radical ($C_6H_{11}^{\bullet}$) (black arrow). From the cycloalkyl peroxide radical ($C_6H_{11}OO^{\bullet}$), cyclohexanone could be generated too through intramolecular elimination of hydroxyl groups ($HO^{\bullet}$) (blue arrow), which was the source of trace cyclohexanone in the oxidation products. Meanwhile, in the CB, the superoxide radical ion ($^{\bullet}O_2^-$) was formed through the reaction between O_2 and electrons (e^-), which was then transformed to H_2O_2 in the presence of abundant C–H bonds and H^+ (red arrow). The hydroxyl radical ($^{\bullet}OH$) generated from decomposition of H_2O_2 could abstract H atoms from C–H bonds to form carbon centred radicals ($C_6H_{11}^{\bullet}$), which would be transformed to cyclohexyl hydroperoxide ($C_6H_{11}OOH$) and cyclohexanone ($C_6H_{10}O$) through the same way in the VB. Through mechanism research, the detailed process of photocatalytic oxidation of C–H bonds with O_2 under irradiation of visible light utilizing T(4-COOH)PP as the photocatalyst, and the sources of oxidation products had been clearly demonstrated, which would provide a solid foundation for further designing efficient and sustainable photocatalysts for C–H bond oxidation. And in the conversion level of mmol ($g_{cat.}^{-1}$ h^{-1}), the generated $^{\bullet}OH$ radicals reacted with the abundant sp^3 C–H bonds around them first, which ensured the stable existence of insoluble porphyrins and metalloporphyrins in this work.

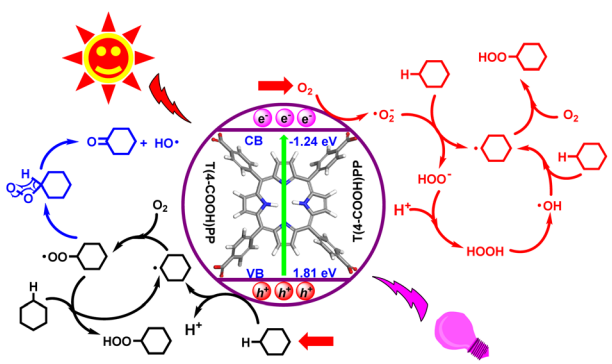

Fig. 10 Speculated reaction mechanism in photocatalytic oxidation of C–H bonds utilizing cyclohexane as the model substrate.

4. Conclusions

An efficient, sustainable and practical strategy for photocatalytic oxidation of C–H bonds with O_2 was developed in this work through learning from nature and utilizing the model compounds of chlorophyll (porphyrins and metalloporphyrins) as photocatalysts. All the representative cycloalkanes and alkyl aromatics could be transformed to their oxygen-containing products at a millimole level (mmol ($g_{cat.}^{-1}$ h^{-1})) under irradiation of visible light at room temperature and solvent-free conditions. For the optimized photocatalyst tetrakis(4-carboxyphenyl)porphyrin (T(4-COOH)PP), the substrate conversion in the model reaction of cyclohexane oxidation reached up to 3.18 mmol ($g_{cat.}^{-1}$ h^{-1}) with the selectivity of 99.9% towards cyclohexyl hydroperoxide. Both of the substrate conversion and selectivity towards oxygen-containing products were higher than that reported in current literature. And the excellent catalytic performance of T(4-COOH)PP was mainly attributed to its higher visible-light absorption, charge separation, production of photo-generated electrons, and lower impedance during charge migration under irradiation of visible light. In this photocatalytic system developed for C–H bond oxidation, not only satisfying substrate compatibility was obtained in which the substrate conversion exhibited higher correlation with the dissociation energy of C–H bonds but also the optimized photocatalyst T(4-COOH)PP could be recycled and reused five times without an obvious decrease in catalytic performance. The main reactive species involved in the reaction

had also been determined as photogenerated electrons (e^-), holes (h^+), superoxide radical ions ($^{\bullet}O_2^-$), hydroxyl radicals ($^{\bullet}OH$), alkyl carbon centred free radicals ($C_6H_{11}^{\bullet}$) and alkyl peroxide radicals ($C_6H_{11}OO^{\bullet}$), based on which the mechanism in this study was speculated. The insertion of an oxygen atom into C–H bonds utilizing visible light as the energy source and T(4-COOH)PP as the photocatalyst developed in this work provided an efficient, sustainable, rational and practical strategy for oxidation of C–H bonds and could act as an important reference for the development of efficient, low-energy consumption, low-carbon emission and sustainable catalytic process, eventually promoting the realization of green chemistry, energy conservation & emission reduction and sustainable development in the chemical industry.

Author contributions

Yan-Bo Ding: data curation; formal analysis; investigation; methodology; writing – review & editing. Yi-Lin Chu: validation; visualization; writing – review & editing. Qiu-Ping Liu: investigation; methodology; writing – review & editing. Hong-Ke Wu: investigation; methodology; writing – review & editing. Hai-Min Shen: conceptualization; data curation; formal analysis; funding acquisition; investigation; methodology; project administration; resources; software; supervision; validation; visualization; roles/writing – original draft; writing – review & editing. Yuan-Bin She: funding acquisition; project administration; resources; supervision.

Conflicts of interest

There are no conflicts to declare.

Data availability

All the data supporting this study are available within the paper and SI. See DOI: https://doi.org/10.1039/d5su00471c.

Acknowledgements

This work was supported by the National Natural Science Foundation of China (grant no. 22178322, 22478353, and 21878275).

References

1 S. Wei, K. X. Li, S. Zhong, R. R. Zhang, G. S. Wang and R. X. Liu, *ACS Appl. Mater. Interfaces*, 2024, **16**, 7252–7264.
2 M. D. Xu, Y. L. Yu, G. J. Shi, P. M. Jian, X. Hou and E. X. Yuan, *ACS Appl. Nano Mater.*, 2024, **7**, 11952–11964.
3 S. X. Chen, B. He, Y. W. Li, R. R. Wang, P. Chen, X. A. Li and R. X. Liu, *Chem. Eng. J.*, 2024, **488**, 150865.
4 J. L. Song, M. L. Hua, X. Huang, J. Ma, C. Xie and B. X. Han, *ACS Catal.*, 2023, **13**, 4142–4154.
5 W. H. Wang, N. Z. Shang, J. M. Wang, X. H. Nie, C. C. Du, X. Zhou, X. Cheng, W. Gao, X. Liu, J. Y. Huang, Y. Q. Qiao, S. T. Gao and C. Wang, *Green Chem.*, 2022, **24**, 6008–6015.
6 A. Vomeri, M. Stucchi, A. Villa, A. B. Hungria, J. Calvino and L. Prati, *ChemCatChem*, 2024, **16**, e202400709.
7 X. J. Li, S. Q. Hao, Z. P. Chen, T. Huang, S. J. Fu, F. F. Zhao, K. Y. You and H. A. Luo, *Ind. Eng. Chem. Res.*, 2024, **63**, 6087–6099.
8 D. G. Montjoy, E. A. K. Wilson, H. R. S. Hou, J. D. Graves and N. A. Kotov, *Nat. Commun.*, 2023, **14**, 857.
9 K. Wang, S. S. Li, J. L. Wang, Z. H. He, D. Wang, R. R. Zhang, W. T. Wang, Y. Yang and Z. T. Liu, *Catal. Today*, 2023, **409**, 42–52.
10 A. Rogolino, J. B. G. Filho, L. Fritsch, J. D. Ardisson, M. A. R. da Silva, G. A. Diab, I. F. Silva, C. A. F. Moraes, M. R. Forim, M. Bauer, T. D. Kühne, M. Antonietti and I. F. Teixeira, *ACS Catal.*, 2023, **13**, 8662–8669.
11 H. Z. Zhang, W. F. Zhong, Q. B. Gong, P. F. Sun, X. Z. Fei, X. J. Wu, S. Xu, Q. H. Zhang, G. Fu, S. J. Xie and Y. Wang, *Angew. Chem. Int. Ed.*, 2023, **62**, e202303405.
12 H. Yin, Y. Y. Yuan, Y. B. Li, J. Tang, W. Z. Zhong and L. Q. Mao, *Green Chem.*, 2023, **25**, 2757–2770.
13 S. Wei, H. Li, K. X. Li, R. R. Zhang, G. S. Wang and R. X. Liu, *Ind. Eng. Chem. Res.*, 2022, **61**, 17842–17853.
14 J. N. Zhao, H. N. Sun, Y. Lu, J. N. Li, Z. Y. Yu, H. F. Zhu, C. F. Ma, Q. W. Meng and X. J. Peng, *Green Chem.*, 2022, **24**, 8503–8511.
15 H. Li, Y. W. Li, R. R. Wang, S. Zhong, R. R. Zhang and R. X. Liu, *Ind. Eng. Chem. Res.*, 2023, **62**, 8754–8766.
16 R. A. Sheldon, *Green Chem.*, 2017, **19**, 18–43.
17 S. L. Y. Tang, R. L. Smith and M. Poliakoff, *Green Chem.*, 2005, **7**, 761–762.
18 S. Y. Tang, R. A. Bourne, M. Poliakoff and R. L. Smith, *Green Chem.*, 2008, **10**, 268–269.
19 K. X. Li, Y. M. Liu, S. Wei, B. He, R. Y. Yan, R. R. Zhang and R. X. Liu, *J. Colloid Interface Sci.*, 2025, **677**, 756–768.
20 K. Wang, Y. Wang, D. Wang, Y. X. Du, X. P. Li, Z. H. He, H. Wang, W. T. Wang, Y. Yang and Z. T. Liu, *Appl. Surf. Sci.*, 2025, **680**, 161447.
21 Z. Y. Zhang, M. Hu, Q. F. Gui, J. Gu, W. L. Xu, Q. B. Xiao and W. Huang, *Chem. Eng. J.*, 2023, **467**, 143501.
22 V. K. Yadav, K. Y. Chauhan and T. Das, *Ind. Eng. Chem. Res.*, 2023, **62**, 20170–20188.
23 J. Yuan, Z. W. He and H. B. Zhang, *J. Catal.*, 2023, **423**, 34–49.
24 H. L. Zhou, C. Guo, S. Q. Zhou, J. He, L. Jiang, Y. J. Chen, Z. Y. Yan, D. M. Chen and J. Q. Wang, *J. Environ. Chem. Eng.*, 2024, **12**, 114487.
25 G. Xu, Y. Zhang, P. X. Liu, Q. F. Deng, Y. Y. Ma, C. L. Zuo and S. K. Ma, *J. Photochem. Photobiol., A*, 2024, **452**, 115578.
26 H. L. Zhou, Y. Shao, Z. Z. Zhou, Y. Yang, J. He, L. Jiang, D. M. Chen, Y. J. Chen, Z. Y. Yan and J. Q. Wang, *Appl. Surf. Sci.*, 2023, **622**, 156957.
27 G. Xu, Y. Zhang, P. X. Liu, Y. Ning, Y. P. Zhao, Q. F. Deng, Y. Y. Ma, C. L. Zuo and S. K. Ma, *Colloids Surf., A*, 2024, **703**, 135391.
28 J. L. Wang, K. Wang, T. Sun, Y. Wang, Z. H. He, H. Wang, W. T. Wang, Y. Yang and Z. T. Liu, *Mol. Catal.*, 2024, **565**, 114400.
29 C. Y. Fu, J. H. Du, N. Shi, L. M. Yang, Q. L. Che and P. F. Zhang, *Sci. Rep.*, 2024, **14**, 17947.

30 B. Rawat, V. R. Battula, P. K. Nayak, D. Ghosh and K. Kailasam, *ACS Appl. Mater. Interfaces*, 2023, **15**, 53604–53613.
31 K. Wang, D. Wang, X. Y. Zhang, J. L. Wang, S. L. Lv, Z. H. He, H. Wang, W. T. Wang, Y. Yang and Z. T. Liu, *Appl. Surf. Sci.*, 2023, **617**, 156600.
32 G. Xu, Y. Zhang, D. D. Peng, D. H. Sheng, Y. Tian, D. Ma and Y. Zhang, *Appl. Surf. Sci.*, 2021, **536**, 147953.
33 J. Zheng, J. C. Liu, X. Y. Feng, Y. J. Luo, W. Cai, Z. W. Liao and Y. X. Fang, *J. Alloys Compd.*, 2025, **1010**, 177367.
34 J. L. Wang, K. Wang, Z. H. He, T. Sun, R. J. You, J. G. Chen, W. T. Wang, Y. Yang and Z. T. Liu, *Dalton Trans.*, 2023, **52**, 476–486.
35 J. L. Wang, K. Wang, Z. H. He, R. R. Zhang, P. F. Guo, W. T. Wang, Y. Yang and Z. T. Liu, *Appl. Surf. Sci.*, 2022, **584**, 152606.
36 G. F. Ji, L. Zhao, Y. F. Wang, Y. Tang, C. He, S. T. Liu and C. Y. Duan, *ACS Catal.*, 2022, **12**, 7821–7832.
37 Y. H. Wang, Q. M. Yang, P. J. Walsh and E. J. Schelter, *Org. Chem. Front.*, 2022, **9**, 2612–2620.
38 Q. L. Li, T. Song, Y. P. Zhang, Q. Wang and Y. Yang, *ACS Appl. Mater. Interfaces*, 2021, **13**, 27323–27333.
39 M. Kotkowiak, A. Dudkowiak and L. Fiedor, *Angew. Chem. Int. Ed.*, 2017, **56**, 10457–10461.
40 C. A. Karg, S. J. Wang, N. Al Danaf, R. P. Pemberton, D. Bernard, M. Kretschmer, S. Schneider, T. Zisis, A. M. Vollmar, D. C. Lamb, S. Zahler and S. Moser, *Angew. Chem. Int. Ed.*, 2021, **60**, 22578–22584.
41 S. Matsubara, S. Shoji and H. Tamiaki, *Chem. Commun.*, 2024, **60**, 12513–12524.
42 S. W. Zhang, D. J. Heyes, L. L. Feng, W. L. Sun, L. O. Johannissen, H. T. Liu, C. W. Levy, X. M. Li, J. Yang, X. L. Yu, M. Lin, S. J. O. Hardman, R. Hoeven, M. Sakuma, S. Hay, D. Leys, Z. H. Rao, A. W. Zhou, Q. Cheng and N. S. Scrutton, *Nature*, 2019, **574**, 722–726.
43 W. C. C. Lee and X. P. Zhang, *Nat. Chem.*, 2023, **15**, 1499–1500.
44 H. S. Wang, Y. W. Ren, X. Feng and H. F. Jiang, *ChemCatChem*, 2024, **16**, e202400119.
45 H. M. Abd El-Lateef, T. N. A. Eskander, M. S. H. Alzubi, M. M. Khalaf and M. A. A. A. El-Remaily, *Curr. Org. Chem.*, 2024, **28**, 463–471.
46 S. W. Ke, W. Li, Y. M. Gu, J. Su, Y. F. Liu, S. Yuan, J. L. Zuo, J. Ma and P. He, *Sci. Adv.*, 2023, **9**, eadf2398.
47 Y. Zhang, X. L. Feng, J. Y. Ni, B. Fu, H. M. Shen and Y. B. She, *Biomimetics*, 2024, **9**, 272.
48 J. Y. Ni, Y. B. Ding, J. Sun, H. K. Wu, H. M. Shen and Y. B. She, *Catal. Commun.*, 2024, **187**, 106876.
49 Y. Zhang, B. Fu, J. Sun, Y. B. Ding, H. M. Shen and Y. B. She, *Mol. Catal.*, 2024, **557**, 113957.
50 X. Y. Zhou, B. Fu, W. D. Jin, X. Wang, K. K. Wang, M. Wang, Y. B. She and H. M. Shen, *Biomimetics*, 2023, **8**, 325.
51 A. B. Guo, J. W. Qin, K. K. Wang, Q. P. Liu, H. K. Wu, M. Wang, H. M. Shen and Y. B. She, *Mol. Catal.*, 2023, **535**, 112853.
52 J. Y. Ni, B. He, H. Huang, L. Ning, Q. P. Liu, K. K. Wang, H. K. Wu, H. M. Shen and Y. B. She, *Mol. Catal.*, 2023, **540**, 113027.
53 H. M. Shen, A. B. Guo, Y. Zhang, Q. P. Liu, J. W. Qin and Y. B. She, *Chem. Eng. Sci.*, 2022, **260**, 117825.
54 H. M. Shen, X. Wang, H. Huang, Q. P. Liu, D. Lv and Y. B. She, *Chem. Eng. J.*, 2022, **443**, 136126.
55 H. M. Shen, M. Y. Hu, L. Liu, B. Qi, H. L. Ye and Y. B. She, *Appl. Catal., A*, 2020, **599**, 117599.
56 H. M. Shen, L. Liu, B. Qi, M. Y. Hu, H. L. Ye and Y. B. She, *Mol. Catal.*, 2020, **493**, 111102.
57 H. M. Shen, B. Qi, M. Y. Hu, L. Liu, H. L. Ye and Y. B. She, *Catal. Lett.*, 2020, **150**, 3096–3111.
58 H. M. Shen, X. Wang, L. Ning, A. B. Guo, J. H. Deng and Y. B. She, *Appl. Catal., A*, 2021, **609**, 117904.
59 H. M. Shen, H. L. Ye, J. Y. Ni, K. K. Wang, X. Y. Zhou and Y. B. She, *Chem. Eng. Sci.*, 2023, **270**, 118472.
60 X. Y. Feng, J. C. Liu, J. Zheng, Y. J. Luo, W. Cai, Z. W. Liao and Y. X. Fang, *J. Organomet. Chem.*, 2024, **1018**, 123304.
61 F. F. Jia, Y. T. Liu, X. W. Deng, X. Cao, X. B. Zheng, L. Y. Zhou, J. Gao and Y. J. Jiang, *ACS Appl. Mater. Interfaces*, 2023, **15**, 7928–7938.
62 D. D. Peng and Y. Zhang, *Appl. Catal., A*, 2023, **653**, 119067.
63 K. Deekamwong, Y. Wada, Y. Y. Zhu, P. M. Usov, Y. Tagami, H. Ohtsu and M. Kawano, *ChemCatChem*, 2023, **15**, e202201288.
64 Q. H. Zhang, B. An, Y. Lei, Z. X. Gao, H. A. Zhang, S. Xue, X. Jin, W. A. Xu, Z. H. Wu, M. B. Wu, X. Yang and W. T. Wu, *Angew. Chem. Int. Ed.*, 2023, **62**, e202304699.
65 C. C. Diniz, O. A. Chaves, H. G. Bonacorso, Y. G. Kappenberg, P. C. Piquini and B. A. Iglesias, *Dyes Pigments*, 2025, **238**, 112715.
66 M. Wilms, D. Tibben, I. Lyskov, S. P. Russo, J. van Embden, E. Della Gaspera, T. U. Connell and D. E. Gómez, *J. Phys. Chem. C*, 2024, **128**, 15041–15047.
67 M. J. Frisch, G. W. Trucks, H. B. Schlegel, G. E. Scuseria, M. A. Robb, J. R. Cheeseman, G. Scalmani, V. Barone, G. A. Petersson, H. Nakatsuji, X. Li, M. Caricato, A. V. Marenich, J. Bloino, B. G. Janesko, R. Gomperts, B. Mennucci, H. P. Hratchian, J. V. Ortiz, A. F. Izmaylov, J. L. Sonnenberg, D. Williams-Young, F. Ding, F. Lipparini, F. Egidi, J. Goings, B. Peng, A. Petrone, T. Henderson, D. Ranasinghe, V. G. Zakrzewski, J. Gao, N. Rega, G. Zheng, W. Liang, M. Hada, M. Ehara, K. Toyota, R. Fukuda, J. Hasegawa, M. Ishida, T. Nakajima, Y. Honda, O. Kitao, H. Nakai, T. Vreven, K. Throssell, J. A. Montgomery Jr, J. E. Peralta, F. Ogliaro, M. J. Bearpark, J. J. Heyd, E. N. Brothers, K. N. Kudin, V. N. Staroverov, T. A. Keith, R. Kobayashi, J. Normand, K. Raghavachari, A. P. Rendell, J. C. Burant, S. S. Iyengar, J. Tomasi, M. Cossi, J. M. Millam, M. Klene, C. Adamo, R. Cammi, J. W. Ochterski, R. L. Martin, K. Morokuma, O. Farkas, J. B. Foresman and D. J. Fox, *Gaussian 16, Revision C.01*, Gaussian, Inc., Wallingford CT, 2019.
68 D. D. Peng, Y. Zhang and X. M. Huang, *J. Alloys Compd.*, 2022, **928**, 167217.

69 Q. L. Li, T. Song, Y. P. Zhang, Q. Wang and Y. Yang, *ACS Appl. Mater. Interfaces*, 2021, **13**, 27323–27333.
70 K. Wang, B. Xue, J. L. Wang, Z. H. He, X. Y. Zhang, S. S. Li, W. T. Wang, Y. Yang and Z. T. Liu, *Mol. Catal.*, 2021, **505**, 111530.
71 J. Zheng, J. C. Liu, X. Y. Feng, J. R. Liu, S. Zong, L. L. Liu and Y. X. Fang, *J. Colloid Interface Sci.*, 2023, **651**, 304–318.
72 X. H. Wang, X. H. Wang, J. F. Huang, S. X. Li, A. Meng and Z. J. Li, *Nat. Commun.*, 2021, **12**, 4112.
73 S. L. Lv, K. Wang, S. S. Li, X. P. Li, T. L. Dang, Z. H. He, H. Wang, W. T. Wang, Y. Yang and Z. T. Liu, *Appl. Catal., A*, 2024, **674**, 119604.